Plant Methods

RESEARCH

Open Access

Nondestructive detection of saline-alkali stress in wheat (*Triticum aestivum* L.) seedlings via fusion technology

Ying Gu[1,2], Guoqing Feng[2], Peichen Hou[2], Yanan Zhou[2], He Zhang[2,3], Xiaodong Wang[2], Bin Luo[2*] and Liping Chen[1,2*]

Abstract

Background Wheat (*Triticum aestivum* L.) is an important grain crops in the world, and its growth and development in different stages is seriously affected by saline-alkali stress, especially in seedling stage. Therefore, nondestructive detection of wheat seedlings under saline-alkali stress can provide more comprehensive technical support for wheat breeding, cultivation and management.

Results This research focused on moisture signal prediction and classification of saline-alkali stress in wheat seedlings using fusion techniques. After collecting and analyzing transverse relaxation time and Multispectral imaging (MSI) information of wheat seedlings, four regression models were used to predict the moisture signal. K-Nearest Neighbor (KNN) and Gaussian-Naïve Bayes (GNB) models were combined with fivefold cross validation to classify the prediction of wheat seedling stress. The results showed that wheat seedlings would increase the bound water content through a certain mechanism to enhance their saline-alkali stress. Under the same Na concentration, the effect of alkali stress on moisture, growth and spectrum of wheat seedlings is stronger than salt stress. The Gradient Boosting Decision Regression Tree model performs the best in predicting wheat moisture signals, with a coefficient of determination (R2P) of 0.98 and a root mean square error of 109.60. It also had a short training time (1.48 s) and an efficient prediction speed (1300 obs/s). The KNN and GNB demonstrated significantly enhanced predictive performance when classifying the fused dataset, compared to using single datasets individually. In particular, the GNB model performing best on the fused dataset, with Precision, Recall, Accuracy, and F1-score of 90.30, 88.89%, 88.90%, and 0.90, respectively.

Conclusions Under the same Na concentration, the effects of alkali stress on water content, spectrum, and growth of wheat were stronger than that of salt stress, which was more unfavorable to the growth of wheat. The fusion of low-field nuclear magnetic resonance and MSI technology can improve the classification of wheat stress, and provide an effective technical method for rapid and accurate monitoring of wheat seedlings under saline-alkali stress.

Keywords Low-field nuclear magnetic resonance, Multispectral imaging, Wheat seedlings, Saline-alkali stress, Nondestructive testing

*Correspondence:
Bin Luo
luob@nercita.org.cn
Liping Chen
chenlp@nercita.org.cn
Full list of author information is available at the end of the article

Graphical Abstract

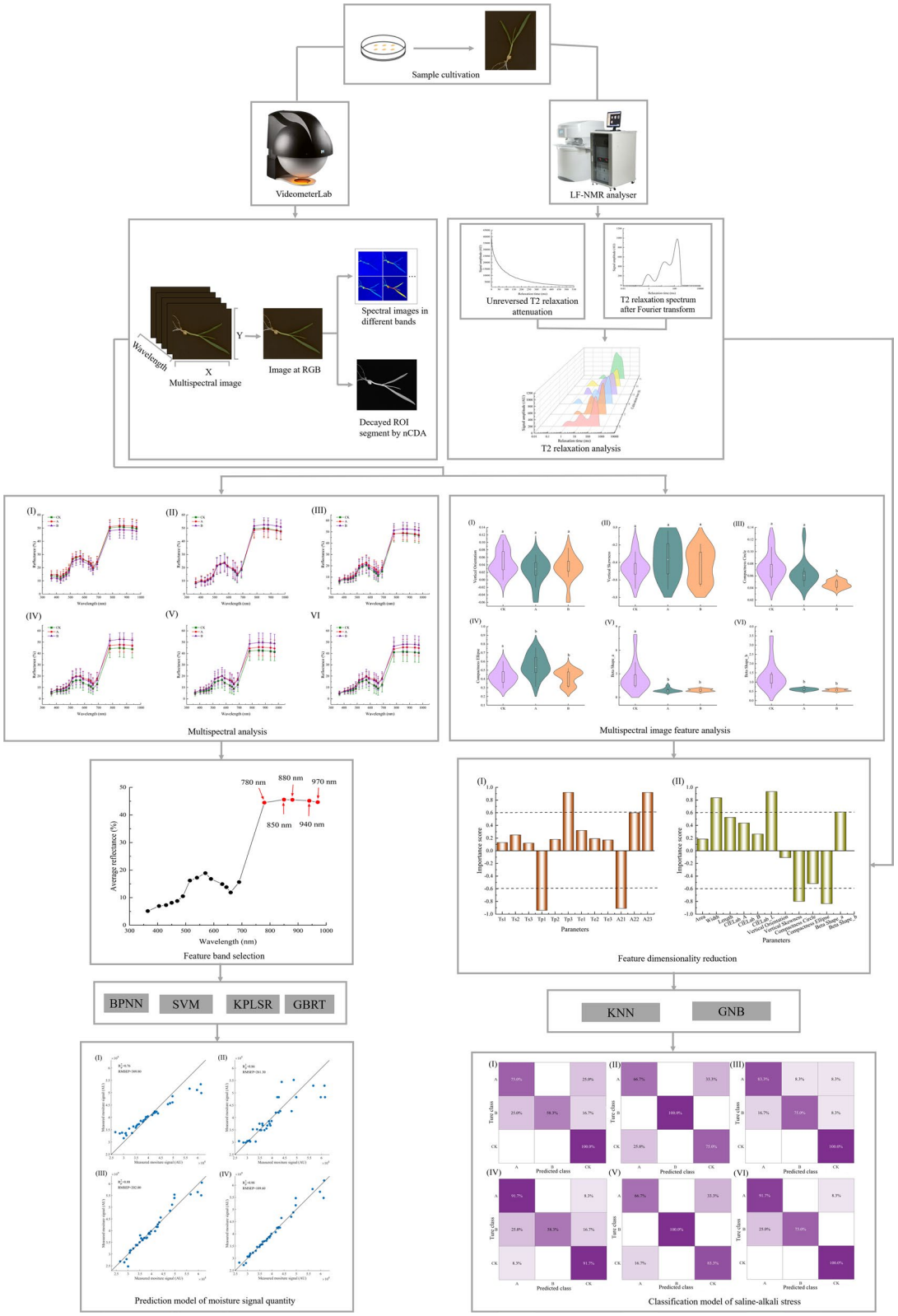

Introduction

Saline-alkali stress caused by soil salinization, as a prominent abiotic stressor, has a detrimental impact on crop growth, consequently affecting global agricultural economy [14, 25, 40]. Globally, over 1 billion hectares of land are affected by soil salinity, with more than 2 million hectares added annually [32, 50]. Wherein, as an important food crop, wheat (*Triticum aestivum* L.) is also facing the negative effects of saline-alkali stress [19, 49]. Saline-alkali stress leads to excessive accumulation of salt and alkaline substances in soil, which affects the growth and physiological metabolism of wheat seedlings, and then affects the yield and quality of crops. In China, most wheat regions are in the period of soil salinity return following the emergence of wheat seedlings, and the soil salt content reaches the maximum. The wheat seedling stage is the weakest stage of saline-alkali stress in wheat life, and the stress at this time has a significant impact on the growth of wheat seedlings [39]. Therefore, accurate and nondestructive detection of wheat seedling response to saline-alkali stress is of great significance for effectively evaluating crop growth status and formulating reasonable saline alkali resistance strategies.

In the existing studies, traditional physiological and biochemical analysis methods are usually used to detect and evaluate the growth status of crops under saline alkali stress [22, 36]. For example, the growth status of crops is evaluated by measuring chlorophyll content, membrane permeability, soluble sugar content, proline content and other indicators [9, 33]. These methods with high accuracy and specificity can directly reflect the physiological and biochemical state of crops, and are of great value for understanding the mechanism of crop response to saline alkali stress and formulating corresponding management measures [36]. However, these methods have some limitations in reflecting crop response, such as destructive, time-consuming and laborious, and unable to carry out continuous monitoring [13]. Therefore, it is very important to seek an accurate, rapid and nondestructive technical method to monitor crops under saline-alkali stress.

In this context, this study combined low-field nuclear magnetic resonance (LF-NMR) and multispectral imaging (MSI) technology to achieve the nondestructive detection of wheat seedling moisture signal and prediction of saline-alkali stress. LF-NMR is a fast, accurate and nondestructive method, which uses the spin relaxation characteristics of hydrogen nuclei in the magnetic field to explain the distribution and migration of water in the sample [6, 26, 30]. Moreover, MSI is a newly developed technology that combines spectroscopy and traditional imaging to simultaneously gather spectral and spatial information [46]. They were developed to measure the morphological characteristics of the inspected objects initially and have been widely used for crop visualization [31]. The fast, accurate, and nondestructive characteristics of LF-NMR and MSI technologies have all crop stakeholders eagerly awaiting the introduction of these novel detection techniques to boost crop productivity overall. LF-NMR provides the moisture content and distribution state of crops from the microscopic perspective, while MSI technology provides a wider range of spectral information, which can reflect the overall growth state of crops. By combining the two technologies, we aim to fill the existing technical gap in the field of crop growth state assessment under saline-alkali stress, and provide a new and efficient monitoring method for crop growth status.

The study involved the following three purposes: (1) To analyze the moisture phase state and multispectral information of wheat seedlings under saline-alkali stress by LF-NMR and MSI technology, and explore the application potential of two nondestructive detection methods under saline-alkali stress in wheat. (2) To carry out the regression prediction of moisture signal quantity of wheat seedlings under saline-alkali stress based on MSI data, and compare the performance of different regression models in predicting moisture signal amplitude. (3) To classify wheat seedlings under different saline-alkali stress through different models, and evaluate the performance of different models in the accuracy of sample classification by fusing LF-NMR and MSI datasets. This work provided a new insight into monitoring the wheat growth status under saline-alkali stress, and the combination LF-NMR and multispectral imaging opened up new possibilities for improving crop resistance to multiple environmental stresses.

Materials and methods

Plant material and experimental design

The experimental wheat material used in this research was Jimai 22, which is widely planted in China. The experimental samples were screened in terms of similar size, quality, with no surface damage. Before the experiment, the wheat was disinfected with 75% alcohol for 5 min and rinsed 3 times with distilled water. Wheat seeds were treated with different stress treatments from the germination stage. After 5 days of germination, the wheat was transplanted into a black hydroponics box with different stress treatment solutions for culture. On the basis of previous studies, the concentration with high stress and low mortality was selected, and the concentration suitable for saline-alkali stress identification in wheat seedling stage was 100 mmol/L [20]. Three experimental treatments were set as control (CK, distilled water), A [100 mmol/L neutral salt (NaCl: Na_2SO_4 = 9:1, pH = 6.68)], and B [100 mmol/L alkaline salt ($NaHCO_3$: Na_2CO_3 = 9:1, pH = 8.9)], and there were

four replications for each treatment. The wheat seedlings were incubated in an MGC Series Intelligent Light incubator (MGC-450BP-2L, Shanghai Yiheng Scientific Instruments Co., Ltd., Shanghai, China) at 25 ± 1 °C with 80% relative humidity and 12 h/12 h alternating light and dark period. Relevant indicators of different treatment groups of wheat were collected every 2 days.

T2 acquisition and processing

The LF-NMR instrument (AniMR, Shanghai Newmark Electronic Technology Co., Ltd., Shanghai, China) was used to collect the transverse relaxation time (T2) of LF-NMR. The basic parameters of the instrument were as follows: Magnetic field intensity: (0.25 ± 0.05) t; Resonance frequency: 8.5–12.8 MHz; Magnetic field uniformity: less than 10 ppm (ϕ60 mm × 100 mm); Magnet temperature: 32℃; Probe coil diameter: 15 mm. The Carr–Purcell–Meiboom–Gill (CPMG) sequence pulse sequence in the NMR spectrum analysis software was used to determine the T2 of the sample. According to the previous test results [7, 15], the main sampling parameters were set as follows: 90° hard pulse width (P1) = 8 μs; 180° hard pulse width (P2) = 12 μs; Sampling frequency(SW) = 200 kHz; Analog gain (RG1) = 43.5 db; Digital gain (DRG1) = 3; Number of signal sampling points (TD) = 907,218; Repeated sampling times (NS) = 16; Waiting time for repeated sampling (TW) = 5000 μs; Echo number (NECH) = 18,000.

The LF-NMR spectrum analysis is a quantitative analysis and detection method using the spectral signal obtained by the Fourier transform of NMR signal. The CPMG collected from the experiment was imported into NMR spectrum inversion software, and the Simultaneous Iterative Reconstruction Technique (SIRT) was used for inversion operation. T2 was obtained after inversion. The inversion parameters were set as follows: minimum relaxation time: 0.01 ms; Maximum relaxation time: 10,000; Number of participating inversion points: 200; Number of iterations: 10,000. In order to eliminate the influence of inconsistent initial quality of test samples on the test results, all signal amplitude data were normalized, and then the data were imported into SPSS 23 for one-way analysis of variance. The OriginPro 2022 was used for drawing in this paper. During the test, the collection of CPMG was repeated three times, and the average value was taken. CPMG of wheat seedlings were collected on the 5th, 7th, 9th, 11th and 15th day of seedling growth. The instrument would be calibrated before each collection, and the water on the sample surface would be wiped gently with absorbent paper to avoid moisture affecting the results (Fig. 1).

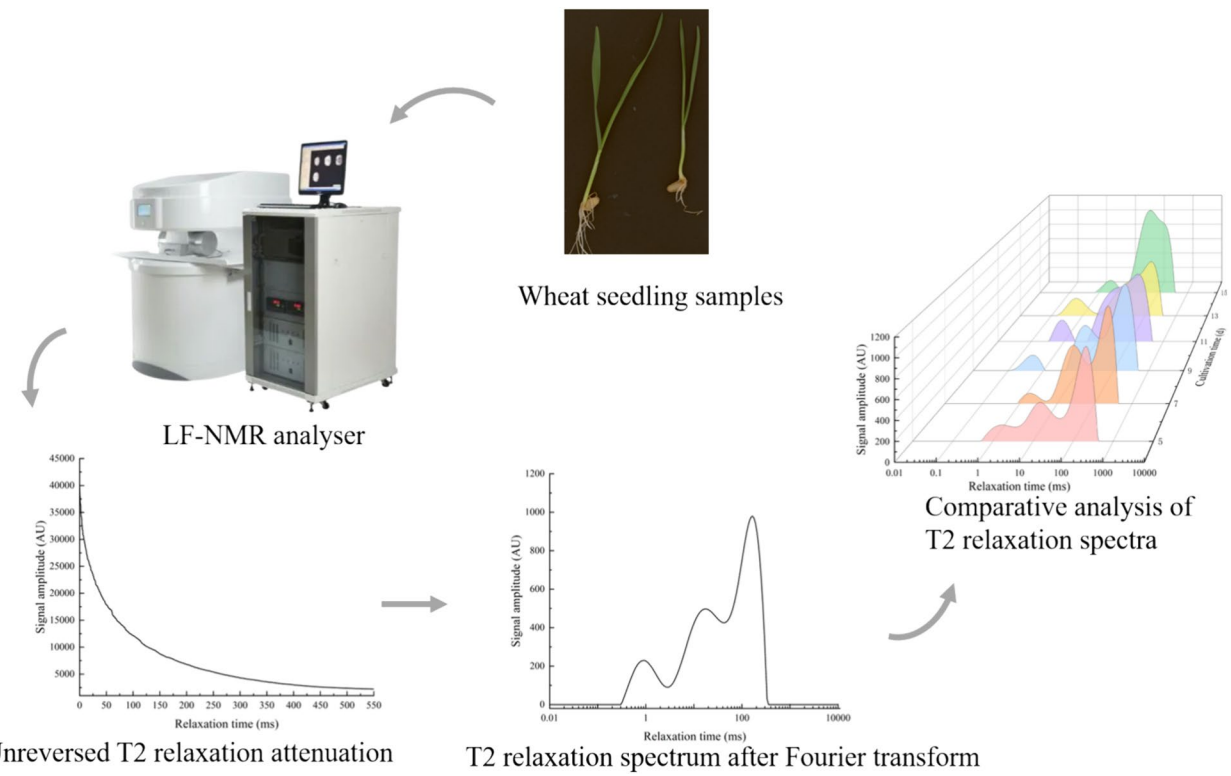

Fig. 1 T2 relaxation data acquisition and analysis process

Multispectral image acquisition and processing

The multispectral images of all wheat seedling samples were taken by a VideometerLab 4 instrument (Videometer A/S, DK-2700 Herlev, Hørsholm 12B, 3.sal, Denmark). The instrument consists of a sphere containing 19 light emitting diodes in the wavelengths 375, 405, 435, 450, 470, 505, 525, 570, 590, 630, 645, 660, 700, 780, 850, 870, 890, 940 and 970 nm. All images were acquired in one sequence, with a resolution of 4096 × 3000 pixels, and a pixel size of 0.03 mm per pixel. Surface reflectance was recorded by the involvement of a standard monochrome charge coupled device chip [45]. Before acquiring multispectral images, the system was fully calibrated radiometrically and geometrically by using three successive plates: a white one for reflectance correction, a dark one for background correction and a doted one for geometric pixel position aligning calibration, followed by a light setup calibration [15, 23].

The multispectral images obtained contained not only wheat seedlings but also some other interference, such as the background board and surrounding debris (Fig. 2). Therefore, it was necessary to remove these objects before extracting the spectral information of individual wheat seedlings. The images were processed using Videometerlab software version 3.22. Background removal in images of complete wheat seedlings was achieved through Normalized Canonical Discriminant Analysis (nCDA), and the seedlings were segmented using a simple threshold. Morphological traits and main spectral features were then extracted from the segmented wheat seedling images. The morphological traits were divided into shape features, color features, and binary features. The shape features included BetaShape_a, BetaShape_b, Compactness Circle, Compactness Ellipse, Vertical Orientation, and Vertical Skewness; color features included CIELab_A, CIELab_B, and CIELab_L; binary features included Area, Length, and Width. The interpretation of morphological shapes was listed in the supplementary file: Supplementary material.

The extracted spectral features represented the average intensity of reflected light at each single wavelength, calculated from all the wheat seedling pixels in the images.

Determination of germination index

The 450 wheat seeds were selected and evenly divided into 9 groups. Each kind of solution (CK, A, and B) was used to cultivate 3 groups of seeds individually. Before the experiment, the wheat was disinfected with 75% alcohol for 5 min and then rinsed three times with distilled water. The wheat seeds were placed on germination paper that had been moistened with an adequate amount of the corresponding solution, ensuring that both the paper and the seeds were sufficiently dampened. The germination paper was changed daily, and the cultivation environment was maintained as described in "Plant material and experimental design". The number of germinated seeds in each group was recorded daily until the 7th day. The germination rate, germination potential, germination index, and average germination time of the wheat were calculated, with the respective formulas shown below [28].

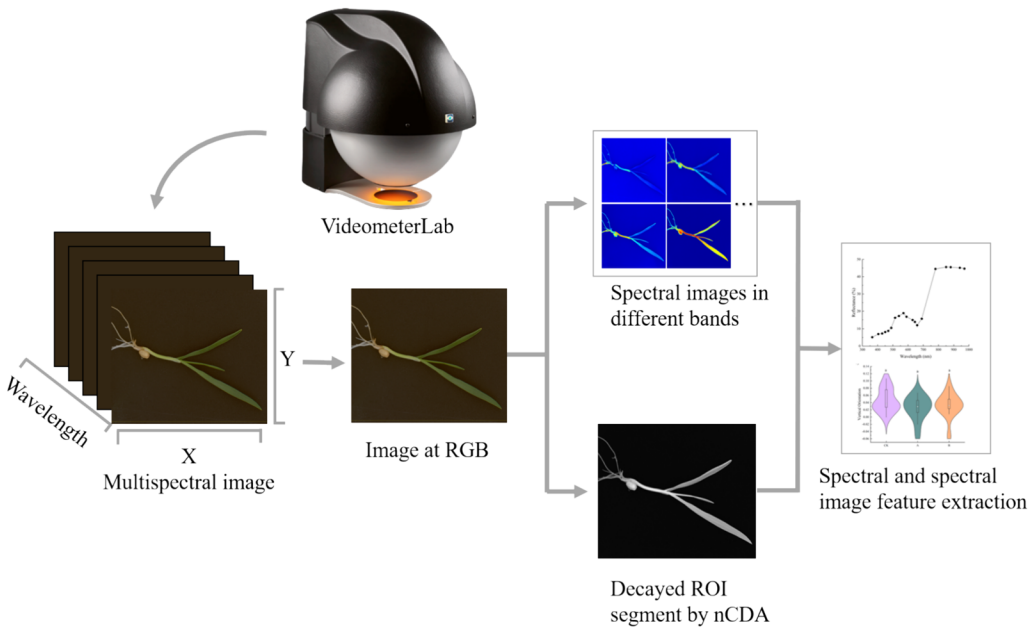

Fig. 2 Multispectral data acquisition and analysis process

$$Germination\ percentage = \frac{Number\ of\ seeds\ germinated}{Total\ number\ seeds} \times 100\%. \quad (1)$$

$$Germination\ potential = \frac{Total\ number\ of\ germinating\ seeds\ on\ day\ 3}{Total\ number\ of\ seed\ samples} \times 100\%. \quad (2)$$

$$Germination\ index = \frac{\sum Gt}{Dt}. \quad (3)$$

$$Average\ germination\ time = \frac{\sum Gt \times Dt}{Number\ of\ seeds\ germinated}. \quad (4)$$

Detection model and performance evaluation

Prediction model of moisture signal quantity

Four regression models including Gradient Boosting Regression Tree (GBRT), Support Vector Machine (SVM), Kernel Partial Least Squares Regression (KPLSR) and Back Propagation Neural Network (BPNN) were established to predict the moisture signal of wheat seedlings under saline-alkali stress using MSI data. Before establishing the quantitative model analysis, the correlation analysis between MSI data and signal amplitude A was established by using Spearman and Kendall algorithm, and the multispectral data with high correlation was selected as the input variable of the model.

For the performance evaluation of the regression model, six evaluation criteria were selected: determination coefficient of training set ($R2_c$), corrected root mean square error (RMSEC), prediction determination coefficient (R2p), prediction root mean square error (RMSEP), training time (s), and predicting speed (obs/s). Wherein, R2 measures the proportion of variation explained by the model in the total variation, and the value range is from 0 to 1; The closer the R^2 value is to 1, the more variation in the data the model explains, indicating better model fitting. In addition, RMSE measures the prediction error of the model on the training set; The smaller the value of RMSE, the better the performance of the model on the training set. The training time and speed reflect the efficiency of the model in practical application. The calculation formula of R2 and RMSE were as follows.

$$R^2 = 1 - \frac{\sum_{i=1}^{n}(y_i - \hat{y}_i)^2}{\sum_{i=1}^{n}(y_i - \bar{y})^2}, \quad (5)$$

$$RMSE = \sqrt{\frac{1}{n}\sum_{i=1}^{n}(y_i - \hat{y}_i)^2}, \quad (6)$$

where i is the data point, n is the number of data points, y_i is the actual value, $\hat{y}_i$ is the predicted value, and $\bar{y}$ the average value of the actual value.

Classification prediction model

In this study, we discussed the application effect of K-Nearest Neighbor (KNN) and Gaussian-Naïve Bayes (GNB) combined with fivefold cross validation method in the classification and prediction model of salt and alkali stress in wheat seedlings. We used three different datasets: MSI datasets, LF-NMR datasets, and fusion datasets of MSI and LF-NMR. At present, KNN and GNB have shown satisfactory results in the field of classification [10].

The prediction performance of the classification model was evaluated by four key indicators: Precision, Recall, Accuracy and F1-score. Precision is the ratio of true positive data to all predicted positive data, indicating the classifier's ability to avoid labeling negative cases as positive. Recall is the ratio of true positive predictions to all actual positive data, indicating the classifier's ability to identify all positive samples. Accuracy is the percentage of samples that are correctly classified by the model, reflecting the overall effectiveness of the classifier on the given dataset. The F1-score is a metric that combines the trade-off between Precision and Recall, providing a single number that reflects the effectiveness of a classifier, particularly in the presence of rare categories. It is calculated as the harmonic mean of Precision and Recall [7, 21]. The four equations of the evaluating indicators were:

$$Precision = \frac{TP}{TP + FP}, \quad (7)$$

$$Recall = \frac{TP}{TP + FN}, \quad (8)$$

$$Accuracy = \frac{TP + TN}{TP + TN + FP + FN}, \quad (9)$$

$$F_1\text{ - score} = \frac{2 \times Precision \times Recall}{Precision + Recall}, \quad (10)$$

where TP, TN, FN, and FP are for true positive, true negative, false negative, and false positive, respectively.

Results

Phenotypic analysis of wheat seedlings under saline-alkali stress

With the increase of culture time, the phenotypic characteristics of wheat seedlings were significantly different between CK, A and B group. The germination rate of CK group reached 95.23% at the 7th day, and the germination potential, germination index and average germination days were significantly different from A and B group (Table 1). From the image, wheat leaves became thin and short due to saline alkali stress, and gradually curl (Fig. 3I). However, when wheat seedlings were cultured to the 9th day, the differences between the groups could not be identified by human eyes. Therefore, we needed to identify whether wheat seedlings were under stress in advance according to multispectral images. Figure 3II showed the multispectral images of wheat seedlings in the bands of 365, 405, 430, 515 and 630 at the 9th day of culture. We could judge the differences of wheat seedlings under different culture conditions according to the multispectral images.

T2 analysis of wheat seedlings under saline-alkali stress

T2 relaxation analysis

The T2 signal amplitude was directly proportional to the water content of living tissues [44]. The T2 relaxation spectra of water in different phases within living crop organs exhibited significant differences, demonstrating the multicomponent nature of the T2 relaxation spectra [6, 47]. Figure 4 is a comparison diagram of T2 relaxation spectra of wheat in the control group (Fig. 4CK), salt stress group (Fig. 4A) and alkali stress group (Fig. 4B) from 5 to 15 days. In Fig. 4, the T2 spectrum of wheat seedlings had three obvious peaks. Considering that the peak positions in the T2 spectrum could reflect the binding energy intensity, the internal water of wheat seedlings was divided into three binding types [12]. The water phases were divided into bound water T21 (0.1 ms < T21 < 1 ms) and signal amplitude A21 from left to right; semi-bound water T22 (1 ms < T22 < 10 ms), signal amplitude A22; free water T23 (10 ms < T23 < 1000 ms), signal amplitude A23. The total signal amplitude was represented by A, i.e., A = A21 + A22 + A23. The contents of A21, A22 and A23 increased as the seedlings matured (Fig. 4). Under stress conditions, the differentiation between A22 and A23 became blurred from the 9th day (Fig. 4A) or the 11th day (Fig. 4B). In addition, compared with the control group, the stress group showed a significant increase in A21.

In this study, the T2 relaxation peak areas of wheat seedlings cultured under three conditions for 15 days were counted and analyzed (Table 2). Within 15 days, the water content of the three phases in all groups increased, but the growth rate was different. From the 5th day to the 7th day, the total water signal volume of CK, A and B groups increased by 312.58%, 221.05% and 149.50%, respectively. During the culture period from the 5th day to the 15th day, the content of A21 in CK group continued to increase by 919.92%, group A increased by 621.64% and group B increased by 494.71%, the A22 of CK A and B groups increased by 1274.35%, 982.94%, and 935.34% in group B, respectively, and the A23 of CK A and B groups increased by 519.91%, 387.49% and 274.84%, respectively. The average growth rates for A21, A22, and A23 were as follows: for A21, B had the highest rate at 171.63%, followed by A at 170.02%, and CK at 168.83%; for A22, the order was CK at 182.27%, A at 180.00%, and B at 164.17%; finally, for A23, CK was highest at 146.71%, followed by A at 131.72%, and then B at 123.32%. Compared with CK group, the average growth rate of bound water in group B was the largest, followed by group A. While the average growth rate of A22 and A23 was the same, which was the largest in group CK, then group A, and finally group B.

Ratio analysis of bound water and free water

From 5th day, the ratio of free water to combined water of wheat seedlings under CK, A and B was carefully tracked (Table 3). The CK group maintained a relatively

Table 1 Comparison of germination of wheat seed under saline-alkali stress

Group	Germination rate (%)	Germination potential (%)	Germination index	Mean germination time (d)
CK	95.23 ± 2.13a	90.21 ± 2.25a	35.51 ± 2.82a	3.15 ± 0.31c
A	70.83 ± 5.71b	62.82 ± 6.67b	18.45 ± 2.42b	4.51 ± 0.44b
B	57.67 ± 8.67c	47.67 ± 10.49c	16.80 ± 3.06b	5.40 ± 0.04a

The data in the table represent the standard errors (± SE) of the four replicates, and different letters of the same column on the table represent significant difference among treatment ($P < 0.05$)

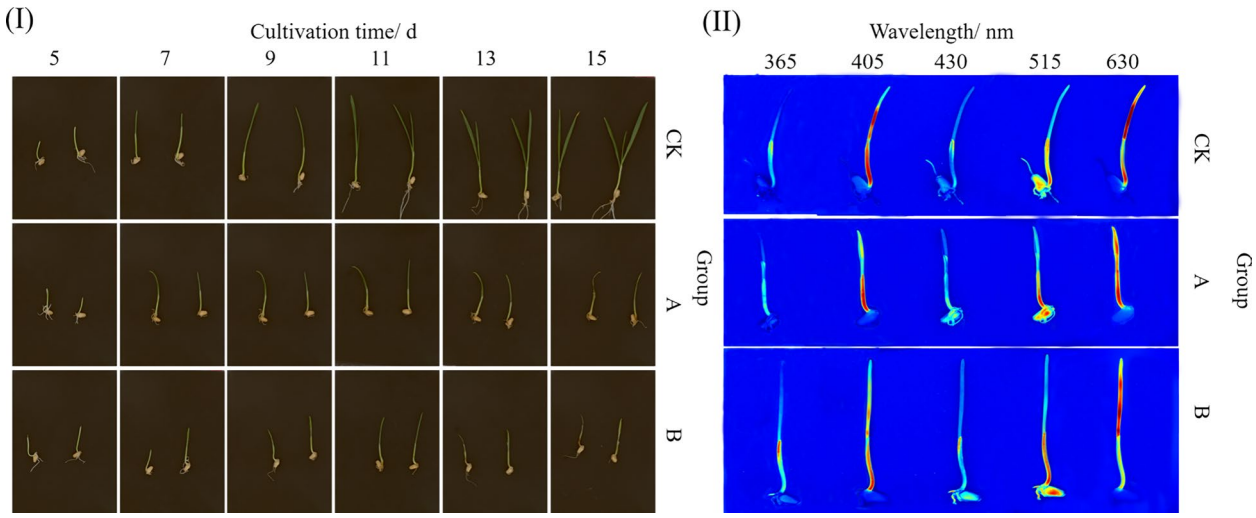

Fig. 3 Effect of saline-alkali stress on phenotypes of wheat seedlings. **I** Phenotypes of wheat seedlings cultured in different environments. **II** Multispectral images of wheat seedlings in various bands at the 9th day of cultivation. CK: control group, A: salt stress, B: alkali stress

stable rate, slightly decreasing from 15.03% on the 5th day to 13.05% on the 15th day. Similarly, within the same period, the A group decreased from an initial 16.01% on the 5th day to 10.28% on the 15th day, while the B group experienced a more significant decrease, from 15.67% to 8.70%. In addition, on the 7th day, the ratio of free water to bound water in the CK group decreased because the seedlings were moved from the Petri dish to the incubator for culture, and the seedlings needed to adapt to changes in the environment. From 7th day to 15th day, the proportion of free water and bound water in the control group and salt stress group began to increase gradually. However, due to salt stress, the ratio of free water to bound water in group A was always lower than that in group CK. On the contrary, the proportion of free water and bound water in group B decreased continuously from the 7th day to the 11th day, and increased from the 13th day, which delayed the adaptation mechanism of wheat seedlings.

MSI analysis of wheat seedlings under saline-alkali stress

Morphological characteristics analysis

Twelve morphological features were extracted from multispectral image. In terms of the average value of shape features, color features and binary features, wheat seedlings growing in different environments were different. For the shape characteristics, the length, width and area of wheat seedlings under saline-alkali stress were significantly different from those of the control group (Fig. 5 I, II, III). The length of wheat seedlings under salt stress and alkali stress had significant difference (Fig. 5I), but the width and area had no significant difference (Fig. 5I, II).

In terms of color characteristics, the CIELab_A color characteristics of wheat seedlings were significantly different between group CK and group B (Fig. 6I). There was no significant difference in the color characteristics of CIELab_B and CIELab_L among the three groups of wheat seedlings (Fig. 6 I, II, III).

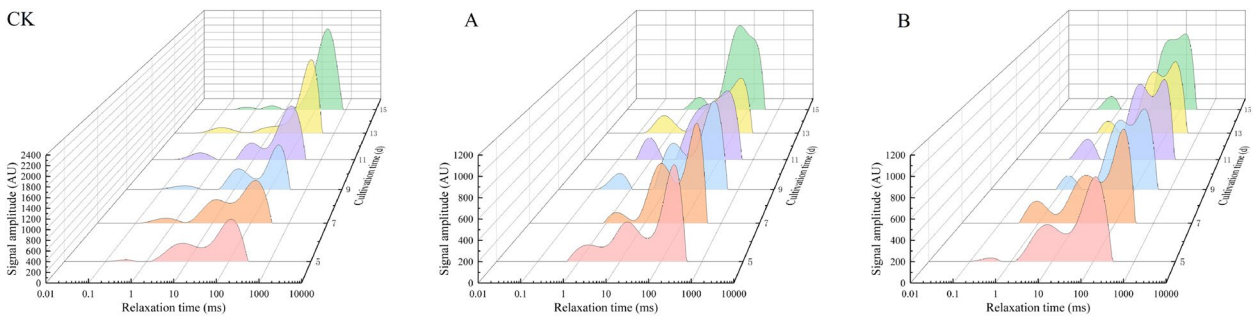

Fig. 4 T_2 inversion spectrum of wheat seedings in three experimental groups

Table 2 Statistics table of unit mass T2 peak area

Group	Cultivation time (d)	Bound water A21	Semi-bound water A22	Free water A23	Total moisture content A
CK	5	698.75 ± 98.11a	2813.10 ± 377.77a	10,502.20 ± 469.54a	12,163.62 ± 662.46a
	7	2779.19 ± 430.84a	7754.66 ± 310.24a	26,371.52 ± 486.72a	38,020.88 ± 488.30a
	9	2955.75 ± 439.26a	10,071.85 ± 673.86a	27,992.63 ± 502.92a	40,380.14 ± 611.06a
	11	3555.39 ± 448.87a	28,053.00 ± 526.44a	35,766.86 ± 477.92a	67,045.94 ± 569.00a
	13	3995.38 ± 405.42a	28,627.49 ± 579.28a	49,205.80 ± 924.32a	81,538.40 ± 579.06a
	15	4291.32 ± 466.49a	35,848.86 ± 654.27a	54,602.19 ± 802.51a	98,608.56 ± 706.14a
A	5	658.47 ± 69.09a	2770.38 ± 168.79a	10,858.96 ± 268.77a	12,290.50 ± 273.15a
	7	2653.78 ± 419.50b	7536.20 ± 449.12a	16,945.62 ± 617.37b	27,168.14 ± 270.88b
	9	2832.63 ± 387.51a	9054.55 ± 782.51a	22,359.99 ± 678.95b	37,567.73 ± 744.61b
	11	3490.34 ± 377.10b	9459.47 ± 617.54b	27,877.75 ± 268.95b	40,861.84 ± 100.63b
	13	3527.46 ± 391.69b	26,389.32 ± 883.99b	32,848.83 ± 594.62b	62,782.03 ± 148.24b
	15	4093.34 ± 418.68b	27,231.07 ± 330.03b	42,077.69 ± 676.71b	73,456.64 ± 832.83b
B	5	701.25 ± 77.51a	2850.95 ± 130.63a	10,985.26 ± 965.09a	13,741.60 ± 273.15a
	7	1919.50 ± 208.89b	4580.33 ± 563.19	14,181.38 ± 121.40c	20,543.35 ± 209.08c
	9	2309.76 ± 397.82b	7289.99 ± 594.83a	16,576.20 ± 141.21c	26,935.96 ± 438.02c
	11	2646.87 ± 339.30c	9358.69 ± 641.68b	18,402.12 ± 357.55c	31,520.49 ± 415.28c
	13	2738.27 ± 353.39c	24,819.55 ± 306.64c	20,017.64 ± 806.29c	47,443.77 ± 278.30c
	15	3469.12 ± 125.59c	26,666.15 ± 369.25c	30,192.27 ± 853.87c	62,631.92 ± 457.72c

All statistical data are unit mass peak area, and to be expressed as mean ± standard deviation ($x \pm s$); different letters stands for significance between gradient groups ($P < 0.05$)

Table 3 The ratio of free water to bound water

Group	Cultivation time (d)					
	5 (%)	7 (%)	9 (%)	11 (%)	13 (%)	15 (%)
CK	15.03	9.49	9.80	10.06	12.32	13.05
A	16.01	7.87	8.18	8.47	9.06	10.28
B	15.67	7.39	7.18	6.95	7.31	8.70

In terms of binary characteristics, there was no significant difference in Vertical Orientation and Vertical Skewness among the three groups (Fig. 7I, II). There were significant differences in the characteristics of Compactness Circle between B and the other groups (Fig. 7III). However, in terms of Compactness Ellipse, Beta Shape_a and Beta Shape_b, there were significant differences between CK and the other groups, but no significant differences between A and B (Fig. 7IV, V, VI).

Multispectral analysis

The average spectral intensity of wheat seedlings was compared to that of a white board to calculate the relative reflection spectrum. Observations of the wheat seedlings began on the 5th day and were conducted every two days, concluding on the 15th day. In general, the average reflectance spectra of CK, A and B groups of wheat seedlings showed a similar trend (Fig. 8). However, with the increase of culture time, the difference between the average reflectance spectra of seedlings in groups A and B and CK gradually increased. When the wavelength was 365 nm (UVA region), the average reflectance spectra of the three groups of wheat seedlings were the minimum in the whole band, and decreased with the growth of seedlings. In the visible region (365–645 nm), the average spectrum showed an "S" type growth. The average spectral value was steep and almost linear in the range from red light to early near infrared (700–780 nm). In the near-infrared region (780–970 nm), the average spectral value tended to be flat. From the 11th day, the average reflectance spectrum of group B was significantly higher than that of the other two groups in 700–780 nm.

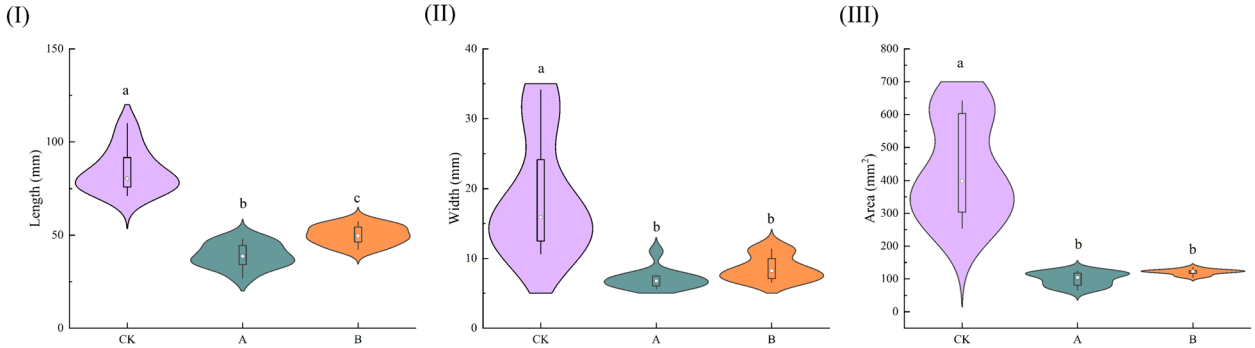

Fig. 5 Shape features of wheat seedings in three experimental groups. All statistical data are represented by mean ± standard deviation (*SD*), with different letters representing the significance between gradient groups ($P < 0.05$, Student's t-test), and the following graph is the same

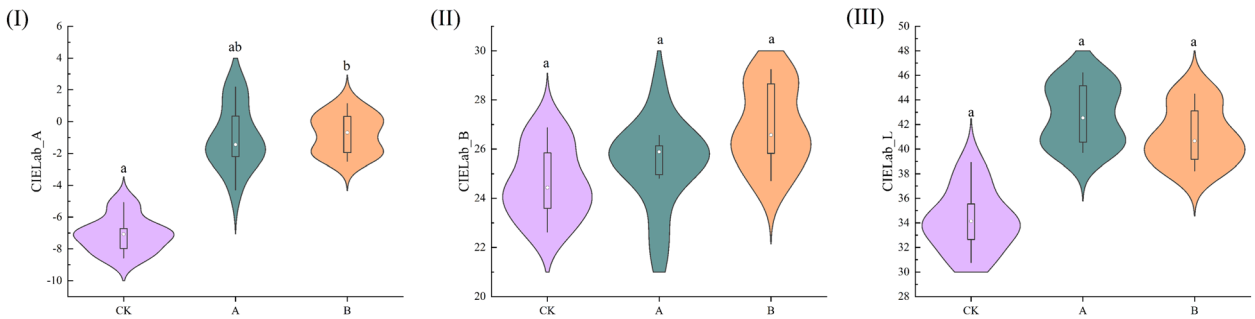

Fig. 6 Color features of wheat seedings in three experimental groups

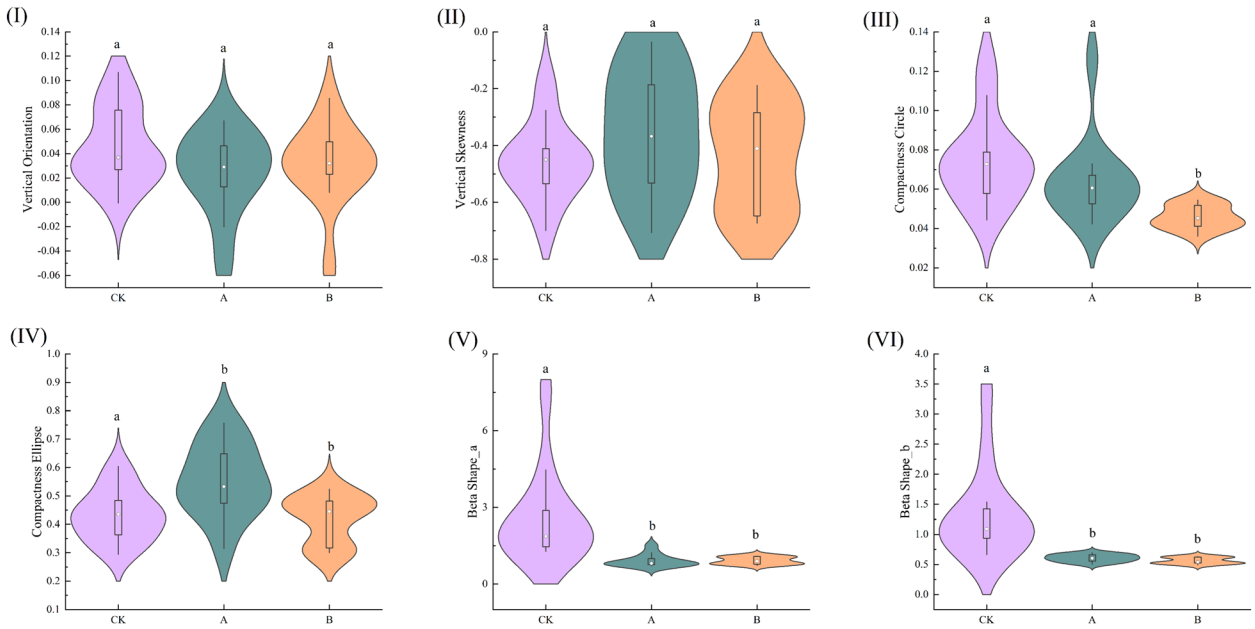

Fig. 7 Binary features of wheat seedings in three experimental groups

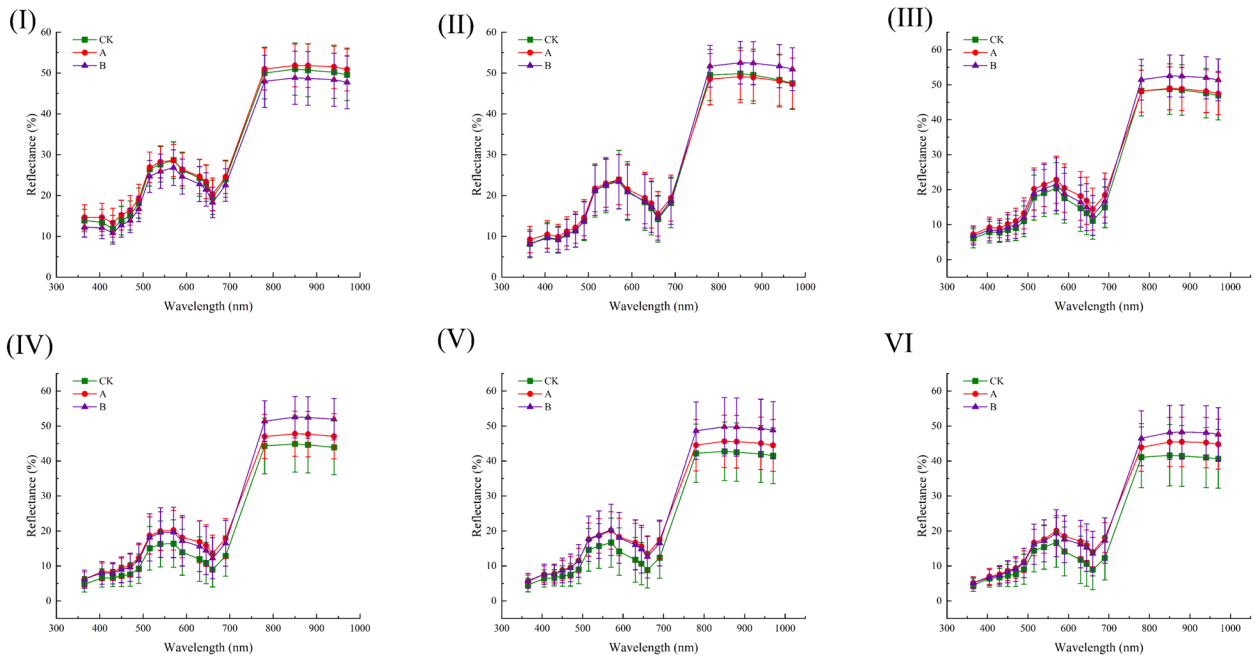

Fig. 8 The average reflectance spectra of wheat seedlings under different treatments were obtained using multispectral imaging system. **I**–**VI** represent wheat seedlings cultured for 5, 7, 9, 11, 13, 15 days, respectively. (CK) control group, (A) salt stress, and (B) alkali stress. Error bar indicate means ± standard deviation (*SD*)

Estimating moisture signal with MSI

Feature parameter selection

Spearman and Kendall correlation analyses were conducted to assess the relationship between the signal quantity of T2 relaxation peak A and the spectral reflection intensity of each band, as detailed in Table 4. At a significance level of $P < 0.05$, the 14 characteristic wavelengths were selected by both methods. At a more stringent significance level of $P < 0.01$, the 5 characteristic wavelengths (780 nm, 850 nm, 880 nm, 940 nm, and 970 nm) were identified (Fig. 9). The 5 wavelengths associated with signal amplitude A and its correlation at a significance level of $P < 0.01$, were selected for use in the modeling process.

The characteristic changes in the electromagnetic radiation absorbed by crops in the near-infrared region (780–2526 nm) were primarily attributed to the stretching and bending vibrations of O–H bonds in water molecules and other molecules. Consequently, alterations in leaf water status could induce corresponding spectral changes in these regions [11, 24, 38, 46].

Table 4 Table of correlation between A parameters and reflectance spectra of wheat seedings

Wavelength	Spearman correlation	Kendall correlation	Wavelength	Spearman correlation	Kendall correlation
365	− 0.53*	− 0.38	630	− 0.57*	− 0.37
405	− 0.33	− 0.27	645	− 0.57*	− 0.37
430	− 0.41	− 0.29	660	− 0.61*	− 0.40
450	− 0.49	− 0.33	690	− 0.57*	− 0.35
470	− 0.53*	− 0.34	780	− 0.79**	− 0.78**
490	− 0.53*	− 0.35	850	− 0.74**	− 0.73**
515	− 0.42	− 0.28	880	− 0.74**	− 0.73**
540	− 0.42	− 0.28	940	− 0.78**	− 0.77**
570	− 0.50*	− 0.32	970	− 0.79**	− 0.80**
590	− 0.55*	− 0.36	–	–	–

*Significance was identified by Spearman correlation and Kendall correlation analysis ($P < 0.05$)

**Significance was identified by Spearman correlation and Kendall correlation analysis ($P < 0.01$)

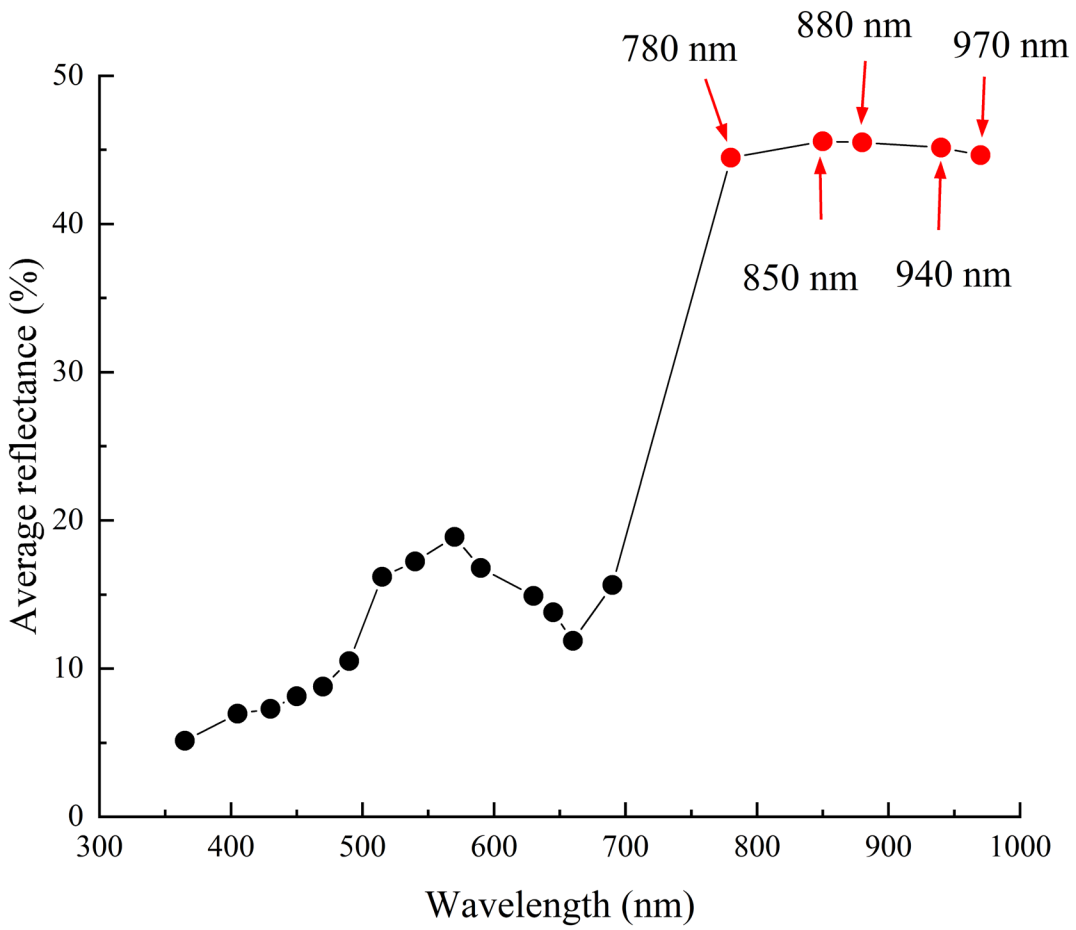

Fig. 9 Selecting characteristic wavelengths related to signal quantity A through correlation analysis

Prediction model analysis

Four regression models (BPNN, SVM, KPLSR, and GBRT) were established to predict the moisture signal A of wheat seedlings under saline-alkali stress using MSI data. The predicted R^2_P values for all models were above 0.75, as detailed in Table 5. Among these models, GBRT demonstrated the best predictive performance, with the R^2_P of 0.98 and the RMSEP of 109.60. Additionally, GBRT had the shortest training time of 1.48 s and the fastest prediction speed of 1300 obs/s. The Fig. 10 illustrated the prediction dataset, highlighting the efficiency of the four models. These results suggested that the combination of MSI and chemometrics could be an excellent non-destructive method for investigating the moisture signal amplitude in wheat seedlings.

Stress prediction using MSI and LF-NMR datasets

Feature parameter selection

The Principal Component Analysis (PCA) was used to reduce the dimension of 9 T2 relaxation parameters, and the Random Forest (RF) was used to reduce the dimension of multispectral image features. The characteristic

Table 5 Performance of the moisture signal amplitude A prediction model using MSI

Model	R^2_C	RMSEC	R^2_P	RMSEP	Training time (s)	Predicting speed (obs/s)
BPNN	0.71	321.60	0.76	309.80	2.09	1900
SVM	0.96	383.90	0.86	261.30	3.34	1800
KPLSR	0.80	332.60	0.88	202.00	6.04	1700
GBRT	0.93	292.2	0.98	109.60	1.48	1300

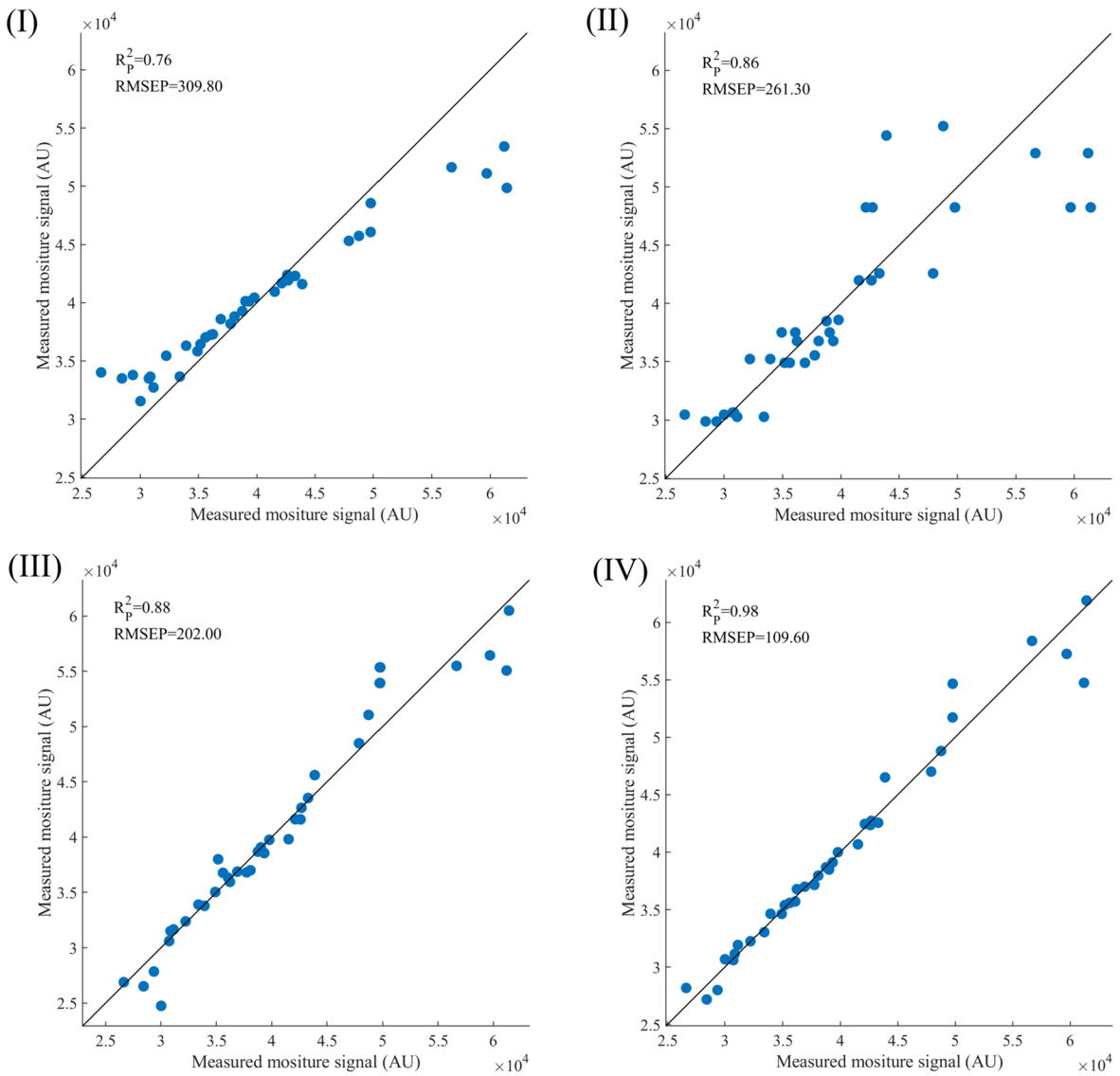

Fig. 10 Use MSI to predict the moisture signal amplitude A. **I** BPNN, **II** SVM, **III** KPLSR, **IV** GBRT

parameters were selected as the input variables of the model according to the importance ranking (Fig. 11). It could be seen from Fig. 11 that PCA selected relaxation parameters (TP1, TP3, A21, A23) with scores greater than 0.6 (Fig. 11I); RF selected characteristic parameters (Width, CIELab_L, Vertical Skewness and Compactness Ellipse) with scores greater than 0.6 (Fig. 11II).

Classification model analysis

In this study, we discussed the application effect of KNN and GNB machine learning models in the classification and prediction of saline-alkali stress in wheat seedlings. We used three different datasets: MSI datasets, LF-NMR datasets, and fusion datasets of MSI and NMR. It could be seen from the confusion matrix that both models could classify wheat seedlings under saline-alkali stress, and the classification accuracy of the fusion dataset of CK group was 100% (Fig. 12). The predicted Recall, Precision, Accuracy and F1-score of the two models for the three test datasets were all above 75.00% (Table 6). In all datasets, GNB model was superior to KNN model in all evaluation indexes, which might be attributed to the advantages of GNB model in processing data with high-dimensional feature space. In addition, the fusion dataset showed better prediction performance on both models, emphasizing the importance of using multi-source data in crop stress prediction.

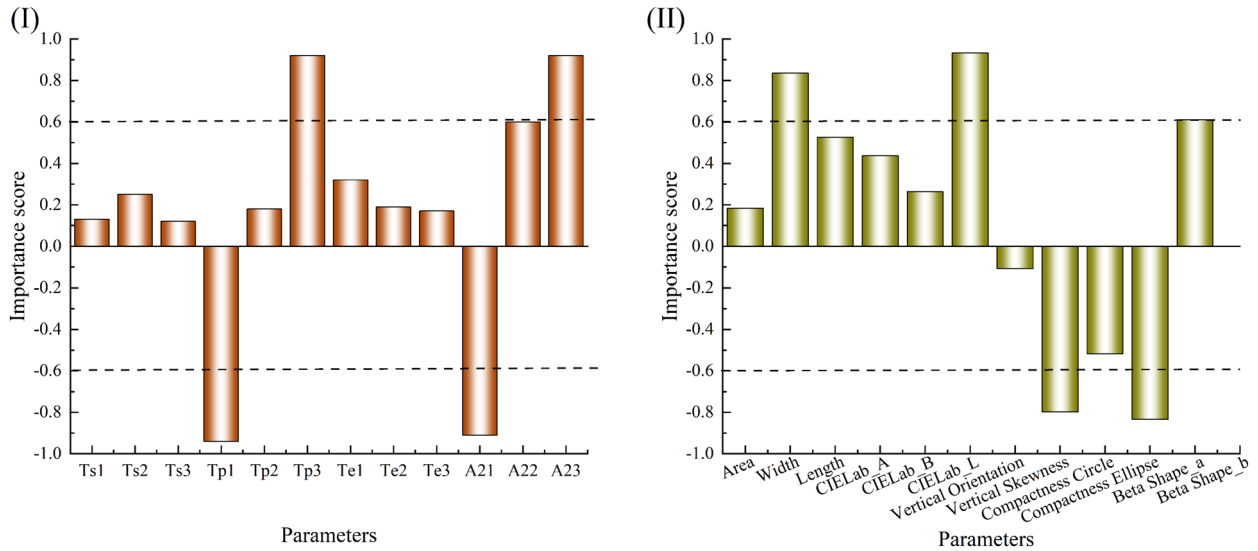

Fig. 11 Selection of relaxation parameters of Principal Component Analysis (PCA) (**I**) and Random Forest (RF) (**II**). Ts1, Ts2, Ts3 is the peak start time; Tp1, Tp2, Tp3, is the peak point to peak time; Te1, Te2, Te3 is the peak end time; A21, A22 and A23 are signal amplitudes

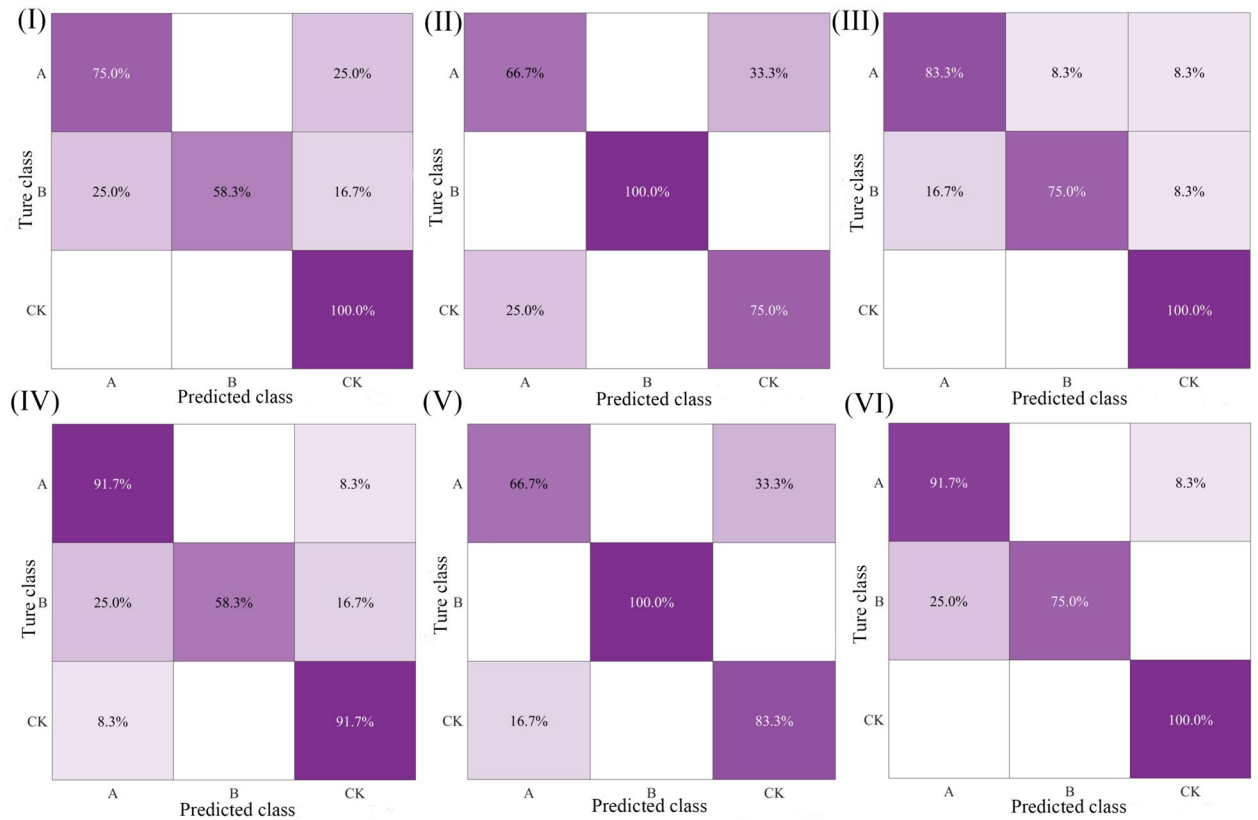

Fig. 12 Confusion matrix of two models on different datasets. **I**–**III** The K-Nearest Neighbor (KNN) model predicts confusion matrices for MSI dataset, LF-NMR dataset, and fusion dataset, respectively; **IV**–**VI** The Gaussian-Naïve Bayes (GNB) model predicts confusion matrices for MSI dataset, LF-NMR dataset, and fusion dataset, respectively

Table 6 The predictive performance of KNN and GNB models

Model	Dataset	Training set				Testing set			
		Precision	Recall	Accuracy	F_1-score	Precision	Recall	Accuracy	F_1-score
KNN	MSI dataset	72.00	72.00	74.00	0.72	81.87	77.76	77.77	0.80
	LF-NMR dataset	76.92	64.52	76.40	0.70	80.47	83.33	80.57	0.81
	Fusion dataset	76.92	72.92	73.63	0.77	86.33	86.11	86.10	0.86
GNB	MSI dataset	72.00	72.00	74.10	0.72	83.97	78.38	80.57	0.82
	LF-NMR dataset	76.92	76.92	76.87	0.77	83.33	80.56	83.33	0.83
	Fusion dataset	73.08	73.08	73.63	0.73	90.30	88.89	88.90	0.90

Discussion

Soil salinization, a prevalent issue in agricultural production, poses a significant challenge to crop cultivation; The saline-alkali stress resulting from soil salinization not only hampers wheat growth but also adversely affects its yield [8]. Traditional research methods, which can damage crops and are time-consuming, often fail to provide continuous monitoring of crops [4, 19]. In this study, we applied salt stress and alkali stress to wheat seedlings and utilized LF-NMR and MSI technology to analyze their responses to saline-alkali stress. This approach demonstrated the potential for accurate and nondestructive detection of crop water status. Furthermore, by employing various regression and classification models, our study not only predicted the quantitative moisture signal amplitude but also achieved qualitative prediction of wheat seedlings under saline-alkali stress.

The germination of wheat seeds was primarily affected by osmotic stress and ion effects caused by salt [27]. Our results showed that, compared to the control group, saline-alkali stress significantly reduced the germination rate, germination potential, and germination index of wheat seeds (Table 1). Analysis of T2 relaxation times revealed that the content of bound water was the lowest among the different types of moisture present. Bound water resided inside wheat cells, combining with proteins through hydrogen bonds. These hydrogen bonds were strong, preventing the free flow of bound water and its participation in metabolic processes. Due to the large hydrogen bonding force, bound water could not move freely within cells and did not engage in metabolism.

Semi-bound water could be adsorbed on other tissues through hydrogen bonding or Coulomb force. Free water which existed in the internal space of wheat by capillary action, had strong fluidity [15, 16]. As a good solvent, free water could dissolve many substances and compounds. The higher the ratio of free water to bound water, the stronger the metabolic activity of seedlings. Under different stress conditions, the ratio of free water to bound water fluctuated, highlighting the complex interaction between environmental stress sources and physiological responses of wheat seedlings. Therefore, during the whole culture period, compared with the control group, the ratio of free water to bound water of seedlings under alkali-stress was the lowest, followed by salt stress group. Both salt stress and alkali stress hindered the increase of water content signal amplitude, and alkali stress played a more significant role. This indicated that alkali stress had a significant effect on the water holding capacity of seedlings (Fig. 4). The results indicated that wheat seedlings could increase the content of bound water through specific mechanisms, thereby enhancing their tolerance to saline-alkali stress in an adverse environment (Table 2). Although all seedlings showed adaptive ability, the efficiency and time of these responses varied with stress types. Compared with alkali stressed seedlings, salt stressed seedlings showed faster recovery in water management (Table 3). Liu et al. [22] draw a conclusion that alkali stress inhibited the growth of wheat more than salt stress at the same Na concentration, which was consistent with the results of this study.

Changes in the water and ion content of wheat exposed to saline-alkali stress could significantly affect its spectral reflectance [5, 5]. This study found that when the wavelength was 365 nm, the average reflectance spectrum was the smallest and decreased with the growth of wheat seedlings. This phenomenon might be related to the increase of phenolic compounds in wheat seedlings. With the growth of seedlings, phenolic compounds would increase [17]. These phenolic compounds (such as flavonoids) had strong absorption capacity in the ultraviolet region [35]. The spectrum at 365–645 nm showed an "S" type growth, this region was mainly related to the absorption peak of crop chlorophyll, which reflected the absorption capacity of crops to photosynthetic effective radiation. In the spectral range of 700–780 nm, the average spectral value was steep and almost linear, which was a typical feature of seedlings [34]. The linear growth meant that with the growth of crops, the leaf structure became more mature and thicker, and the light

scattering ability was enhanced. In the spectral range of 780–970 nm, the changes of spectral reflectance were mainly related to the internal structure and water content of leaves. The gentle trend showed that the structure and water state of crop leaves had reached a balance state to a certain extent. In addition, from the 11th day (Fig. 8IV), the average reflectance spectrum in this region of group B was significantly higher than that of the other two groups. This could be due to the alkali stress altering the internal structure and water regulation mechanisms of crop leaves, which in turn affected the reflectance spectrum. Alkali stress might promote the activation of some protective mechanisms, such as the accumulation of osmotic adjustment substances, which helped to maintain the water state of cells, and then affected the spectral reflectance. The photosynthetic characteristics of seedlings under abiotic stress could be used as the best index to determine the ability of crops to deal with saline alkali stress [2]. This study found that under the same Na concentration, the impact of alkali stress on the wheat's spectral characteristics was more pronounced than that of salt stress. As Zhang et al. [48] proposed, multispectral technology could effectively improve the accuracy of stress monitoring.

Long-term continuous monitoring of water status of wheat plants can not only enrich the water transport theory of Soil Plant Atmosphere Continuum (SPAC), but also have important significance in clarifying the adaptation mechanism of crops to the environment, efficient water use and water-saving regulation [42]. However, the traditional moisture detection has the disadvantages of complex operation, harmful chemical reagents to human body, destructive to samples and so on, which is difficult to be widely used [3]. With the rapid development of nondestructive testing technology, researchers began to explore the nondestructive detection of crop moisture. Yang et al. [41] found that there was a consistent linear relationship between nuclear magnetic signal amplitude and moisture content on wet basis during rice seed germination ($R^2=0.98$). Similarly, Yao et al. [43] found that there was a linear relationship between the pure water content of each organ of wheat and the total signal amplitude A of T2 relaxation spectrum ($R^2=0.99$). Therefore, this study predicted the water signal of wheat based on multispectral data. This study selected the multispectral band with high correlation with water to predict the wheat water signal amplitude A. The results showed that GBRT model performed best in quantitative prediction of water signal, with high accuracy and rapid response ability (Fig. 5), which was of great significance for real-time monitoring of crop water status.

Compared with single data source, data fusion significantly improves the performance of prediction model [1]. For example, the collaborative retrieval model of hyperspectral and multispectral images based on double branch convolution network can effectively use the characteristics of data [37]. Compared with the yield estimation model based on single sensor data, multi-source data fusion can effectively improve the estimation accuracy of winter wheat yield [29]. The prediction accuracy of the winter wheat yield estimation model based on multispectral and thermal infrared data fusion was 8% higher than that based on multispectral data alone [18]. Therefore, in terms of qualitative prediction, we compared the performance of a single LF-NMR or MSI data source with the model fused with LF-NMR and MSI data source, and found that the Precision, Recall, Accuracy and F1-score of the model after data fusion were excellent (Fig. 12, Table 6). It confirmed the effectiveness of information fusion in improving the application of precision agriculture, which meant that data fusion could be used to improve the classification and prediction ability of wheat seedlings under different saline alkali stress levels.

The fusion of LF-NMR and MSI technology, this study provided a new perspective for the nondestructive detection and evaluation of wheat seedlings under saline-alkali stress, and also pointed out the direction of future research. Although this study had achieved positive results, there were still limitations. The selected saline alkali stress level might not fully cover the actual field situation, which might limit the universality of the model in a wide range of applications. More saline-alkali stress levels and adding more variety samples could be explored in future research to increase the robustness and generalization ability of the model. In addition, there might be differences between the predicted moisture amplitude signal of NMR and the prediction effect of actual moisture. In this paper, only the NMR signal was used for measurement, and the drying method was not used for actual calibration. After that, a variety of methods would be used to calibrate the predicted data. The relationship between other biological parameters (such as ion absorption, chlorophyll content, etc.) and water status could also be further explored to comprehensively evaluate the response of crops to stress. Finally, the combination of machine learning model and traditional crop growth model might provide a deeper understanding for predicting crop performance in changing environments.

Conclusion

In this study, we combined LF-NMR and MSI technology to achieve nondestructive detection of wheat seedlings under saline-alkali stress. Under stress, wheat seedlings would increase bound water content through specific mechanisms to enhance their saline-alkali stress tolerance. However, the efficiency and timing of these

responses vary with stress types. Compared to alkali stress, salt stress endowed seedlings with a stronger recovery ability in water management. Stress can induce changes in the internal structure and water regulation mechanisms of wheat leaves. The impact of alkali stress on wheat spectral characteristics was more pronounced than that of salt stress. At the same Na concentration, alkaline stress inhibited wheat growth more than salt stress. Model comparison revealed that the GBRT model excelled in predicting wheat moisture signals, with the R^2_P of 0.98 and the RMSEP of 109.60. It also featured a short training time of 1.48 s and a high prediction speed of 1300 obs/s. For qualitative prediction, the KNN and GNB models demonstrated significantly better classification abilities on the fused datasets compared to using only MSI or LF-NMR datasets alone. Notably, the GNB model showed the most outstanding classification prediction effect on the fused dataset, with Precision, Recall, Accuracy, and F1-score of its test set reaching 90.30%, 88.89%, 88.90%, and 0.90, respectively. These findings not only demonstrated the application potential of LF-NMR and MSI information fusion technology in agriculture but also provided an effective method for predicting the moisture signal quantity in wheat seedlings and accurately classifying saline-alkali stress effects.

Supplementary Information

The online version contains supplementary material available at https://doi.org/10.1186/s13007-024-01248-6.

Supplementary Material 1.

Acknowledgements
The authors would like to acknowledge the generous guidance provided by the National Key Research and Development Program of China and the Reform and Development Project of Beijing Academy of Agriculture and Forestry (Research and development of non-destructive testing technology and equipment for wheat and millet spikelet number based on deep learning). The authors would like to thank the editor and anonymous reviewers for their helpful suggestions on the quality improvement in this paper.

Author contributions
Ying Gu: Conceptualization, Investigation, Methodology, Supervision, Software, Data curation, Visualization, Writing—original draft, Writing—review and editing. Guoqing Feng: Methodology, Resources, Data curation, Software. Peichen Hou: Methodology, Resources. Yanan Zhou: Writing—review and editing, Funding acquisition. He Zhang: Visualization, Writing—review and editing. Xiaodong Wang: Methodology, Resources. Bin Luo: Project administration, Funding acquisition, Supervision, Writing—review and editing. Liping Chen: Methodology, Supervision, Writing—review and editing.

Funding
This work was supported by the National Key Research and Development Program of China (No. 2022YFD2002301) and the Reform and Development Project of Beijing Academy of Agriculture and Forestry (Research and development of non-destructive testing technology and equipment for wheat and millet spikelet number based on deep learning).

Data availability
No datasets were generated or analysed during the current study.

Declarations

Ethics approval and consent to participate
All authors agreed to publish this manuscript.

Consent for publication
Not applicable.

Competing interests
The authors declare no competing interests.

Author details
[1]College of Information and Electrical Engineering, Shenyang Agricultural University, Shenyang 110866, China. [2]Intelligent Equipment Research Center, Beijing Academy of Agriculture and Forestry Sciences, Beijing 100089, China. [3]College of Agriculture, Northeast Agricultural University, Harbin 150006, China.

Received: 6 June 2024 Accepted: 27 July 2024
Published online: 05 September 2024

References

1. Alparone L, Arienzo A, Garzelli A. Spatial resolution enhancement of vegetation indexes via fusion of hyperspectral and multispectral satellite data. Remote Sens. 2024;16:875. https://doi.org/10.3390/rs16050875.
2. An Y, Gao Y, Tong SZ, et al. Morphological and physiological traits related to the response and adaption of bolboschoenus planiculmis seedlings grown under salt-alkaline stress conditions. Front Plant Sci. 2021;12: 567782. https://doi.org/10.3389/fpls.2021.567782.
3. Chen M, Li JL, Li W, et al. Dynamic testing and imaging of living maize kernel moisture using low-field nuclear magnetic resonance (LF-NMR). Trans Chin Soc Agric Eng. 2020;36:285–92. https://doi.org/10.11975/j.issn.1002-6819.2020.23.033.
4. Cui M-H, Chen X-Y, Yin F-X, et al. Hybridization affects the structure and function of root microbiome by altering gene expression in roots of wheat introgression line under saline-alkali stress. Sci Total Environ. 2022;835: 155467. https://doi.org/10.1016/j.scitotenv.2022.155467.
5. El-Hendawy S, Al-Suhaibani N, Alotaibi M, et al. Estimating growth and photosynthetic properties of wheat grown in simulated saline field conditions using hyperspectral reflectance sensing and multivariate analysis. Sci Rep. 2019;9:16473. https://doi.org/10.1038/s41598-019-52802-5.
6. Gu Y, Chen Y, Yue X, et al. Effects of 6-Benzylaminopurine on internal water distribution and growth state of soybean. Trans Chin Soc Agric Eng. 2022;38:303–8. https://doi.org/10.11975/j.issn.1002-6819.2022.05.036.
7. Gu Y, Li J, Zhang H, et al. Effect of 6-benzyladenine on soybean seed germination under salt stress and establishment of stress grade prediction model. Plant Stress. 2024;11: 100388. https://doi.org/10.1016/j.stress.2024.100388.
8. Guo B, Lu M, Fan Y, et al. A novel remote sensing monitoring index of salinization based on three-dimensional feature space model and its application in the Yellow River Delta of China. Geomat Nat Haz Risk. 2023;14:95–116. https://doi.org/10.1080/19475705.2022.2156820.
9. Guo R, Yang ZZ, Li F, et al. Comparative metabolic responses and adaptive strategies of wheat (*Triticum aestivum*) to salt and alkali stress. BMC Plant Biol. 2015;15:170. https://doi.org/10.1186/s12870-015-0546-x.
10. Guo Y, Cao H, Han S, et al. Spectral-spatial hyperspectralImage classification with k-nearest neighbor and guided filter. IEEE Access. 2018;6:18582–91. https://doi.org/10.1109/ACCESS.2018.2820043.
11. Guo Z, Zhai L, Zou Y, et al. Comparative study of Vis/NIR reflectance and transmittance method for on-line detection of strawberry SSC. Comput Electron Agric. 2024;218: 108744. https://doi.org/10.1016/j.compag.2024.108744.
12. Hu X, Wu P, Zhang S, et al. Moisture conversion and migration in single-wheat kernel during isothermal drying process by LF-NMR. Drying Technol. 2019;37:803–12. https://doi.org/10.1080/07373937.2018.1459681.
13. Izadi MH, Rabbani J, Emam Y, et al. Effects of salinity stress on physiological performance of various wheat and barley cultivars. J Plant Nutr. 2014;37:520–31. https://doi.org/10.1080/01904167.2013.867980.

14. Ji J, Zhang J, Wang X, et al. The alleviation of salt stress on rice through increasing photosynthetic capacity, maintaining redox homeostasis and regulating soil enzyme activities by Enterobacter sp. JIV1 assisted with putrescine. Microbiol Res. 2024;280:127590. https://doi.org/10.1016/j.micres.2023.127590.
15. Jia C, Wang L, Yin S, et al. Low-field nuclear magnetic resonance for the determination of water diffusion characteristics and activation energy of wheat drying. Drying Technol. 2020;38:917–27. https://doi.org/10.1080/07373937.2019.1599903.
16. Jiang M, Wu P, Xing H, et al. Water migration and diffusion mechanism in the wheat drying. Drying Technol. 2021;39:738–51. https://doi.org/10.1080/07373937.2020.1716001.
17. Jin Z, Xu Y, Wang M, et al. Changes of phenolic compounds and their antioxidant activities during wheat germination. Food Ferment Indus. 2019;45:199–202. https://doi.org/10.13995/j.cnki.11-1802/ts.017617.
18. Lan M, Fei SP, Yu XL, et al. Application of multispectral and thermal infrared data fusion in estimation of winter wheat yield. J Triticeae Crops. 2021;41:1564–72. https://doi.org/10.7606/j.issn.1009-1041.2021.12.15.
19. Li X, Li S, Wang J, et al. Exogenous abscisic acid alleviates harmful effect of salt and alkali stresses on wheat seedlings. Int J Environ Res Public Health. 2020;17:3770. https://doi.org/10.3390/ijerph17113770.
20. Li YY, Chen B, Yao LR, et al. Evaluation of salt and alkali tolerance and germplasm screening of 283 wheat varieties (lines) during germination. J Agric Sci Technol. 2021;23:25–33. https://doi.org/10.13304/j.nykjdb.2020.0203.
21. Liao FB, Feng XQ, Li ZQ, et al. A hybrid CNN-LSTM model for diagnosing rice nutrient levels at the rice panicle initiation stage. J Integr Agric. 2023;23:711. https://doi.org/10.1016/j.jia.2023.05.032.
22. Liu D, Ma Y, Rui M, et al. Is high pH the key factor of alkali stress on plant growth and physiology? A case study with wheat (*Triticum aestivum* L.) seedlings. Agronomy. 2022;12:12081802. https://doi.org/10.3390/agronomy12081820.
23. Liu W, Xu X, Liu C, et al. Rapid discrimination of high-quality watermelon seeds by multispectral imaging combined with chemometric methods. J Appl Spectrosc. 2019;85:1044–9. https://doi.org/10.1007/s10812-019-00757-w.
24. Liu C, Sun PS, Liu SR. A comparison of spectral reflectance indices in response to water: a case study of Quercus aliena var. acuteserrata. Chinese Journal of Plant Ecology. 2017; 41(08): 850-861. https://doi.org/10.17521/cjpe.2016.0095.
25. Lu P, Dai S, Yong L, et al. A soybean sucrose non-fermenting protein kinase 1 gene, GmSNF1, positively regulates plant response to salt and salt-alkali stress in transgenic plants. Int J Mol Sci. 2023;24:12482. https://doi.org/10.3390/ijms241512482.
26. Lyndgaard CH, Kistrup AT, Christine. HB. Determination of dry matter content in potato tubers by low-field nuclear magnetic resonance (LF-NMR). Journal of Agricultural and Food Chemistry. 2010; 58(19): 10300-4. https://doi.org/10.1021/jf101319q.
27. Mourad AMI, Farghly KA, Börner A, et al. Candidate genes controlling alkaline-saline tolerance in two different growing stages of wheat life cycle. Plant Soil. 2023;493:283–307. https://doi.org/10.1007/S11104-023-06232-Y.
28. Nidal F, Ismail M, Abdelhalem M, et al. Phosphate solubilizing rhizobacteria isolated from jujube ziziphus lotus plant stimulate wheat germination rate and seedlings growth. PeerJ. 2021;9:e11583–e11583. https://doi.org/10.7717/PEERJ.11583.
29. Song CY, Geng HW, Fei SP, et al. Study on yield estimation of wheat varieties based on multi-source data. Spectrosc Spectral Anal. 2023;43:2210–9. https://doi.org/10.3964/j.issn.1000-0593(2023)07-2210-10.
30. Song P, Yue X, Gu Y, et al. Assessment of maize seed vigor under saline-alkali and drought stress based on low field nuclear magnetic resonance. Biosys Eng. 2022;220:135–45. https://doi.org/10.1016/j.biosystemseng.2022.05.018.
31. Takhtkeshha N, Mandlburger G, Remondino F, et al. Multispectral light detection and ranging technology and applications: a review. Sensors. 2024;24:1669. https://doi.org/10.3390/s24051669.
32. Tarolli P, Luo J, Park E, et al. Soil salinization in agriculture: mitigation and adaptation strategies combining nature-based solutions and bioengineering. iScience. 2024;27:108830. https://doi.org/10.1016/j.isci.2024.108830.
33. Thakur R, Yadav S. Biofilm forming, exopolysaccharide producing and halotolerant, bacterial consortium mitigates salinity stress in *Triticum aestivum*. Int J Biol Macromol. 2024;262: 130049. https://doi.org/10.1016/j.ijbiomac.2024.130049.
34. Ustin SL, Gitelson AA, Jacquemoud S, et al. Retrieval of foliar information about plant pigment systems from high resolution spectroscopy. Remote Sens Environ. 2009;113:S67–77. https://doi.org/10.1016/j.rse.2008.10.019.
35. Vodnik D, Vogrin Ž, Šircelj H, et al. Phenotyping of basil (*Ocimum basilicum* L.) illuminated with UV-A light of different wavelengths and intensities. Sci Horticult. 2023;309:111638. https://doi.org/10.1016/j.scienta.2022.111638.
36. Wang J, Xie H, Han J, et al. Effect of graphene oxide-glyphosate nanocomposite on wheat and rape seedlings: growth, photosynthesis performance, and oxidative stress response. Environ Technol Innov. 2022;27:102527. https://doi.org/10.1016/j.eti.2022.102527.
37. Wang YZ, Xiao ZY. Hyperspectral and multispectral co-inversion of chlorophyll content in maize leaves based on two-branch convolutional network. Trans Chinese Soc Agric Mach. 2024;55:196–202. https://doi.org/10.6041/j.issn.1000-1298.2024.01.018.
38. Wu D, He Y, Feng S. Short-wave near-infrared spectroscopy analysis of major compounds in milk powder and wavelength assignment. Anal Chim Acta. 2008;610:232–42. https://doi.org/10.1016/j.aca.2008.01.056.
39. Wu D, Zhang F, Sui CY, et al. Exogenous active substances: effect on stress resistance of wheat seedling. Chinese Agric Sci Bull. 2022;38:14–9. https://doi.org/10.11924/j.issn.1000-6850.casb2021-0871.
40. Xiao G, Wang M, Li X, et al. TaCHP encoding C1-domain protein stably enhances wheat yield in saline-alkaline field. J Integr Plant Biol. 2023;66:169. https://doi.org/10.1111/jipb.13605.
41. Yang H, Zhang L, Ji J, et al. Analysis on water absorption of rice seeds during germination process under polyethylene glycol solution using low-field nuclear magnetic resonance. Trans Chinese Soc Agric Eng. 2018;34:276–83. https://doi.org/10.11975/j.issn.1002-6819.2018.17.036.
42. Yang Q, Zhang F, Liu X. Search progress on regulation mechanism for the process of water transport in plants. Acta Ecol Sin. 2011;70:129–46.
43. Yao S, Du G, Mou H, et al. Detection of water distribution and dynamics in body of winter wheat based on nuclear magnetic resonance. Trans Chinese Soc Agric Eng. 2014;30:177–86. https://doi.org/10.3969/j.issn.1002-6819.2014.24.021.
44. Yao S, Mou H, Du G, et al. Water imbibition and germination of wheat seed with nuclear magnetic resonance. Trans Chinese Soc Agric Mach. 2015;46:266–74. https://doi.org/10.6041/j.issn.1000-1298.2015.11.036.
45. Younas S, Mao Y, Liu C, et al. Measurement of water fractions in freeze-dried shiitake mushroom by means of multispectral imaging (MSI) and low-field nuclear magnetic resonance (LF-NMR). J Food Compos Anal. 2020;96:103694. https://doi.org/10.1016/j.jfca.2020.103694.
46. Younas S, Mao Y, Liu C, et al. Measurement of water fractions in freeze-dried shiitake mushroom by means of multispectral imaging (MSI) and low-field nuclear magnetic resonance (LF-NMR). J Food Compos Anal. 2021;96:103694. https://doi.org/10.1016/j.jfca.2020.103694.
47. Yue X, Bai Y, Wang Z, et al. Low-field nuclear magnetic resonance of maize seed germination process under salt stress. Trans Chinese Soc Agric Eng. 2020;36:292–300. https://doi.org/10.11975/j.issn.1002-6819.2020.24.034.
48. Zhang J, Yu H, Dang J. Research on inversion model of wheat polysaccharide under high temperature and ultraviolet stress based on dual-spectral technique. Spectrosc Spectral Anal. 2023;43:2705–9.
49. Zhang K, Tang J, Wang Y, et al. The tolerance to saline-alkaline stress was dependent on the roots in wheat. Physiol Mol Biol Plants. 2020;26:947–54. https://doi.org/10.1007/s12298-020-00799-x.
50. Zhao X, Xi H, Yu T, et al. Spatio-temporal variation in soil salinity and its influencing factors in desert natural protected forest areas. Remote Sens. 2023;15:5054. https://doi.org/10.3390/rs15205054.

Publisher's Note